*Annals of Biomedical Engineering*, Vol. 26, pp. 381–390, 1998
Printed in the USA. All rights reserved.

0090-6964/98 $10.50 + .00


# Mechanical Characterization of an *In Vitro* Device Designed to Quantitatively Injure Living Brain Tissue

BARCLAY MORRISON III,* DAVID F. MEANEY,* and TRACY K. MCINTOSH*†

*Department of Bioengineering and †Department of Neurosurgery, University of Pennsylvania, Philadelphia, PA

*(Received 3 February 1997; accepted 5 September 1997)*

**Abstract—**Due to the nonlinear, viscoelastic material properties of brain, its mechanical response is dependent upon its total strain history. Therefore, a low strain rate, large strain will likely produce a tissue injury unique from that due to a high strain rate, moderate strain. Due to a lack of current understanding of specific *in vivo* physiological injury mechanisms, *a priori* assumptions cannot be made that a low strain rate injury induced by currently employed *in vitro* injury devices is representative of clinical, nonimpact, inertial head injuries. In the present study, an *in vitro* system capable of mechanically injuring cultured tissue at high strain rates was designed and characterized. The design of the device was based upon existing systems in which a clamped membrane, on which cells have been cultured, is deformed. However, the present system incorporates three substantial improvements: (1) noncontact measurement of the membrane deflection during injury; (2) precise and independent control over several characteristics of the deflection; and (3) generation of mechanical insults over a wide range of strains (up to 0.65) and strain rates (up to $15\ s^{-1}$). Such a system will be valuable in the elucidation of the mechanisms of mechanical trauma and determination of injury tolerance criteria on a cellular level utilizing appropriate mechanical injury parameters. © *1998 Biomedical Engineering Society.* [S0090-6964(98)00203-3]

**Keywords—**Cell culture, Mechanical stimulus, Stretch injury, Dynamic loading.

## INTRODUCTION

A great deal of effort has been expended in the development of clinically relevant *in vivo* models of central nervous system (CNS) injury,[9] and a successful *in vitro* model should mimic these models closely while providing data which are normally unobtainable *in vivo*. To date, several different types of *in vitro* devices have been developed to mechanically injure CNS derived cells. To examine mechanisms involved in the post-traumatic sequelae, a plastic stylet has been used to induce physical trauma to cells in a culture well.[31] Lasers have been used to transect single neuronal processes in culture without affecting surrounding cells.[14,19] Others have subjected cells and tissue of various types to either dynamic or quasi-static changes in hydrostatic pressure in an effort to simulate compression trauma.[26,33] Another class of models directly applies a load or acceleration to the cultured cells, thereby causing injury.[3,18,20] Many devices injure cells by deforming the substrate on which the cells have grown; measuring the displacement of the substrate allows for the possible quantification of the strain applied to the cells.[5,7,11] The device described herein is based on such a device with substantial improvements incorporated into its design.

One important piece of information that cannot be measured directly with *in vivo* models is the strain history of the brain during injury. Knowledge of the strain history is particularly crucial in determining injury tolerance criteria as well as in designing safety systems to prevent such injuries. Experimental work with subhuman primates has been able to reproduce clinically relevant injury outcomes including coma as well as axonal terminal clubbing and diffuse axonal damage.[1,6,10,27,30] Attempts to determine tissue strain have generally employed high speed video of physical models filled with surrogate brain material subjected to similar forces as those that caused clinically relevant injuries in subhuman primates. Experimentally measured strains in the physical models were correlated with histological findings, and it was suggested that strains between 0.10 and 0.50 with strain rates on the order of $10–50\ s^{-1}$ were necessary to produce damage.[21,22,24,25] The device described herein is capable of accurately and reproducibly generating deformations at comparable strains and strain rates.

Due to its nonlinear, viscoelastic material properties, the mechanical response of brain tissue to deformation is dependent upon its total strain history.[16,28,34,37] Some currently employed *in vitro* devices injure tissue using a relatively low strain rate ($\epsilon' < 1$), but large strain ($0.31 < \epsilon < 1.70$).[7,23] The mechanical response of a nonlinear, viscoelastic material to a low strain rate deformation will likely be different than its response to a more clinically relevant, high strain rate deformation. It is therefore unlikely that the physiological response of

Address correspondence to Tracy K. McIntosh, Ph.D., 3320 Smith Walk, Hayden Hall, Room 120, Philadelphia, PA 19104. Electronic mail: mcintosh@eniac.seas.upenn.edu

brain tissue to a high strain rate deformation (consistent with *in vivo* injury) has been modeled with fidelity by most currently employed *in vitro* injury devices.

It was the goal of the present work to characterize a device designed to mechanically injure cultured tissue in a manner consistent with loading conditions thought to cause nonimpact, inertial brain injury *in vivo*. The device is presented in detail with a representative selection of mechanical data acquired during an injury. The device description is augmented with a theoretical membrane analysis which allows for the calculation of the strain field throughout the membrane from parameters measured during an experiment, in particular—displacement of the center of the membrane. The data obtained with the device (including strain) is compared to a more detailed, theoretical analysis of the deformation of the membrane. This theoretical analysis of deformation is validated with physical casts of the deformed membrane, while the strain calculations are compared to strain measurements made on a specially marked membrane. Although these data would not be normally available during an experiment, they were vital for establishing the validity of the theoretical calculations describing strain throughout the entire membrane as well as the device output. Although the device is capable of measuring the dynamic displacement of the membrane, due to technical limitations the measurements of membrane strain and generation of casts were made on membranes which had been deformed statically but not dynamically.

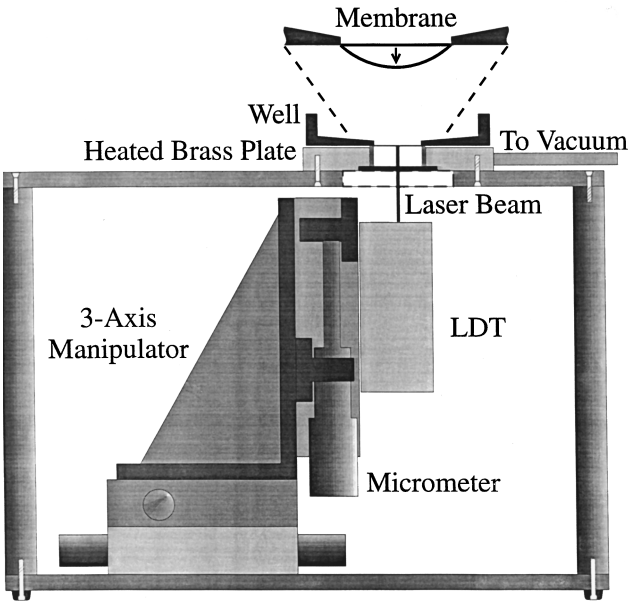


**FIGURE 1. A diagram of the injury device depicting the major components is presented. A laser displacement transducer (LDT) is mounted on a three axis manipulator for centering the laser beam on the membrane. A micrometer in the *z* direction is included for calibration of the LDT. The assembled well, consisting of a silicone membrane held in place on a stainless steel well with an O-ring, is clamped to a heated brass plate forming a pressure chamber. The pressure chamber is connected to two solenoid–needle valve combinations (not shown), which allow for control of the membrane displacement. Tissue or cells are cultured on the top side of the membrane which is displaced downward by a vacuum pulse as depicted in the blow-up illustration. The LDT measures the displacement of the center of the membrane during the injury without affecting its deformation.**

## MATERIALS AND METHODS

The device consists of three separate components: the cell culture well, the base, and the solenoid and needle valves. The cell culture well is comprised of a 60 mm stainless steel well with an 18 mm diameter hole in the center. A sheet of Sylgard membrane, 0.38 mm (0.015 in.) thick (Specialty Manufacturing, Saginaw, MI) is attached to the bottom of the well with an O-ring, thereby sealing the well. Desired cells can be cultured in this well on the exposed Sylgard membrane.

At the time of injury, the well is clamped to a brass plate heated by a thin film resistive heating element (Minco, Minneapolis, MN). A PID (proportional, integral, and derivative) controller (Omega Engineering, Stamford, CT) maintains the well and its contents at 37 °C. The brass plate and well combination form a pressure vessel that is evacuated to deform the membrane (Fig. 1).

A laser displacement transducer (LDT) (Omron Electronics, Schaumburg, IL) is situated beneath the brass plate and is attached to a three-axis manipulator (Newport, Ervine, CA) with a micrometer to measure the displacement in the vertical direction. The LDT consists of a laser light source and a position sensing device (PSD) (Fig. 2). The light is projected to the object, and the diffuse reflection off the object is focused by the lens onto the PSD. Using principles of triangulation, the distance of the object from the sensor is determined and converted to an output voltage. The bottom of the heated brass plate contains a glass window so that the laser beam can strike the underside of the membrane and measure its displacement.

The final component of the system consists of the two solenoid and needle valve combinations which afford fine control over the membrane deformation. One valve controls the duration of the vacuum pulse, which is responsible for the deformation of the membrane, and the second controls the timing and duration that the pressure vessel is allowed to vent. The needle valves, connected to each solenoid valve, control the rate of flow of either the vacuum or the exhaust. All timing events are controlled by a computer outfitted with an analog/digital (A/D) board (ASO-1200 Keithley, Taunton, MA) which is equipped with output as well as input channels. Two of the digital logic output channels are used to activate

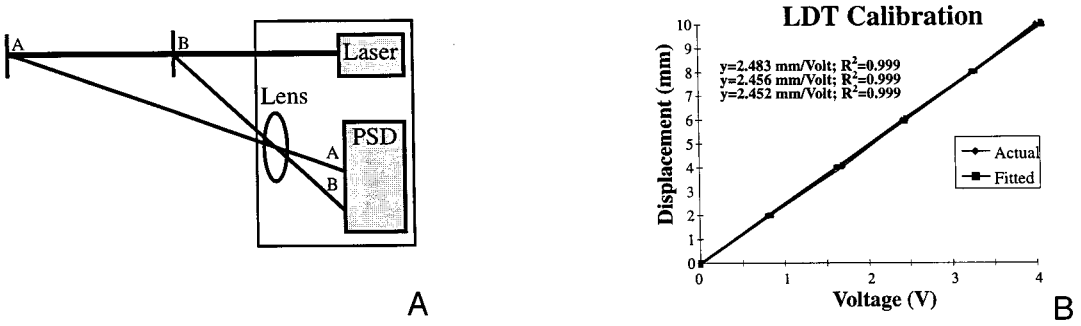


**FIGURE 2. A schematic of the LDT as well as calibration curves are presented. (A) A laser in the sensing head of the LDT spot-illuminates the membrane. The diffuse reflection from the target is focused by a lens onto a position sensing device (PSD). By utilizing principles of triangulation, the distance of the object from the sensing head is calculated and translated into a voltage output. (B) The LDT was calibrated on a membrane which had been statically deformed to three different displacements, 0, 3.3, and 6.1 mm. Voltage readings were acquired every 2 mm over a span of 10 mm for a total of 6 points. A linear equation was then fitted to the voltage readings. The three sets of raw data points and fitted calibration data points are plotted together. Also included in the figure are the slopes of each fitted line as well as the $R^2$ values. As is demonstrated by the similarity of the three calibration curves, the curvature of the membrane does not affect either the linearity of the LDT nor its accuracy.**

cascaded transistor switches, which in turn energize the solenoid valves.

The custom software used to drive the A/D board captured the signal from the LDT and calculated a smoothed displacement trace from the raw displacement data utilizing a Savitzky–Golay smoothing filter, which fit a second order polynomial over a local region of 69 points.[29] From the smoothed displacement data, radial Lagrangian strain at the center of the membrane was calculated from the following formula:

$$\epsilon_{\text{biaxial}} = \frac{2}{3}\left(\frac{w}{a}\right)^2 - \frac{2}{15}\left(\frac{w}{a}\right)^4 + \frac{2}{35}\left(\frac{w}{a}\right)^6,$$

where $w$ is the displacement of the center of the circular membrane and $a$ is the radius of the clamped membrane. The above formula is derived from a simplified geometrical analysis of the deformed membrane, which has been presented in detail by Winston and colleagues.[39] A second Savitzky–Golay filter was used to calculate the strain rate from the strain data.

For each individual well prior to deformation, the beam of the LDT was centered on the clamped circular membrane and then calibrated with the micrometer in the $z$ axis. To calibrate the LDT, readings were obtained every 2 mm over 10 mm for a total of 6 points, and the custom software performed a least squares linear fit to the data points. The coefficients (slope and intercept) were then used to calculate the displacement of the membrane (Fig. 2).

The theoretical strain field over the entire membrane was calculated. At strains of 0.10–0.65, the ratio of membrane thickness to deflection was greater than 3; consequently, the membrane was assumed to deform as a clamped membrane and not as a clamped plate.[4,36,38,39] The circular, clamped membrane was assumed to be isotropic, homogeneous, incompressible, and hyperelastic and to be deformed by a pressure acting normal to the deformed surface. Bending moments throughout the membrane were assumed to be negligible. The complete state of stress and strain in the deformed membrane was represented as a set of nonlinear ordinary differential equations (see the Appendix)[13,15,38] which were numerically solved in MATLAB (The Math Works, Inc., Natick, MA) using an adaptive second order Runge–Kutta procedure.

Measurement of the circumferential strain was also performed on a MicroComputer Imaging Device (MCID) image analysis system (Imaging Research, Ontario, Canada). The MCID system is a general purpose, PC based, image analysis package which allows for image acquisition as well as processing. Concentric rings were transferred to the membrane of an assembled well with a custom aluminum stamp. An image of the stamped membrane was acquired and the distance of each of these rings from the center of the well was measured with the MCID system before and after a static deformation of the membrane. Circumferential strain was calculated as the change in distance of a given ring from the center divided by its original distance. Rings on each membrane were measured three times, and a total of three different membranes were used. Precision of the digitized images and measurements is 30 $\mu$m per pixel. Radial strain was not measured.

Casts of the deformed membrane were made with poly-methyl-methacrylate dental cement. The membrane was deformed a desired amount by evacuating the pressure chamber formed by the well and brass plate. The chamber was sealed so as to maintain a constant vacuum, and a cast of the deformed membrane was made by

filling the open side of the well with dental cement and allowing it to cure. All casts were then cut in half, and the exposed surface ground smooth. Care was taken to ensure that the exposed surface represented a diameter of the circular mold. These casts were digitized using the MCID system, and the images were digitally traced using CorelDraw (Corel, Ottawa, Canada) to produce a line representation of the cast. Precision of the digitized images is 30 $\mu$m per pixel.

## RESULTS

The LDT produced a linear output over the range of interest ($R^2 > 0.99$) as depicted in Fig. 2. After calibration, displacement data for a particular membrane at various system settings was acquired (Fig. 3). The device is capable of producing strains over either a very short [Fig. 3(A)] or an extended period of time [Fig. 3(B)]. The system was successfully engineered to operate over several orders of magnitude to offer flexibility in experimental design.

The device was designed so that the strain rate can be adjusted independently of other parameters associated with the displacement, such as relaxation rate and strain [Fig. 4(A)]. Relaxation rate can be adjusted independently of other parameters associated with the displacement [Fig. 4(B)] as can the duration [Fig. 4(C)]. Figure 3(C) illustrates a 90 ms displacement which can be compared to the 20 ms displacement in Fig. 3(A); all other aspects of the deformation remained identical. The device was found to provide an extremely sensitive degree of control over relevant injury parameters.

To determine the effect of membrane curvature on its accuracy, the LDT was calibrated with the membrane at three separate, static displacements, 0, 3.3, and 6.1 mm. When the membrane is displaced 3.3 mm at its center, it adopts the conformation of a sphere with a radius of 14.0 mm; when the membrane is displaced 6.1 mm at its center, it adopts the conformation of a sphere with a radius of 9.7 mm.[39] The three calibration curves along with the raw data are plotted in Fig. 2. With all of the system settings constant (needle valve settings, vacuum level, and timing), two displacement traces were acquired with each of these calibration factors (data not shown). Parameters of importance from each of the six experimental traces are summarized as mean $\pm$ standard deviation (SD): strain $= 0.15 \pm 0.007$, strain rate $= 16.38 \pm 0.70$, and relaxation rate $= 14.39 \pm 0.39$.

The theoretical radial and circumferential ($\lambda_1$ and $\lambda_2$, respectively) stretch ratios across the membrane radius were calculated for center stretch ratios of 1.25 [Fig. 5(A)] and 1.65 [Fig. 5(B)], which correspond to center displacements of 5.5 and 8.0 mm, respectively. Circumferential stretch ratios were measured and have been incorporated into Fig. 5. The simplified, geometrical for-

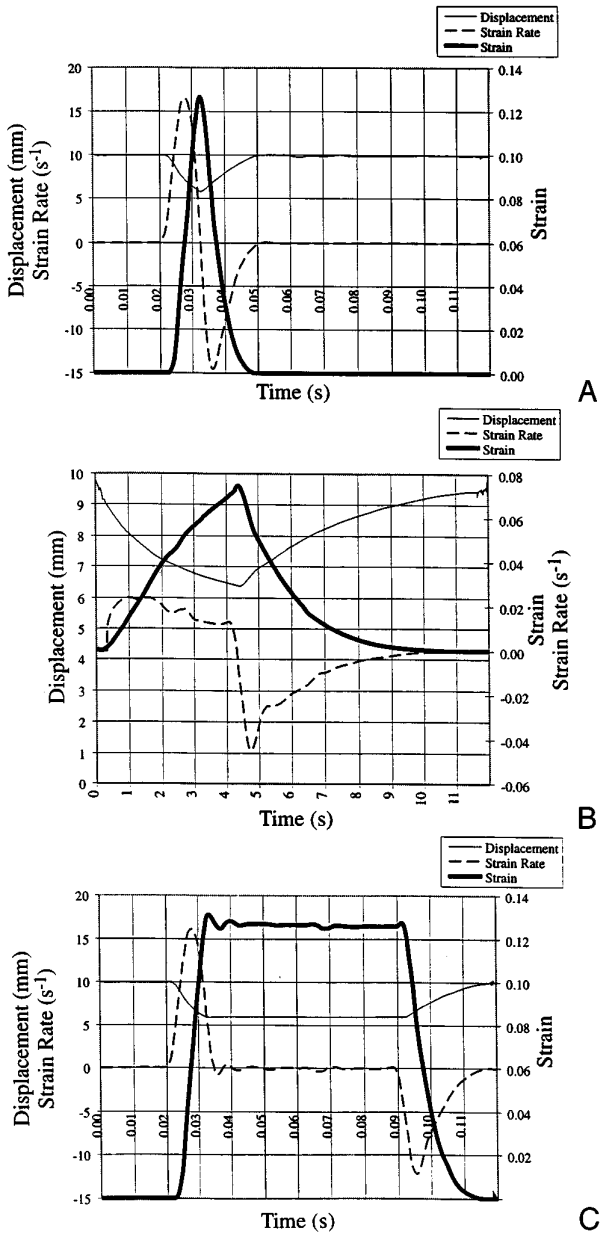


**FIGURE 3. Displacement, strain, and strain rate data acquired from three experiments at different settings. (A) Data from an experiment with a displacement lasting 20 ms with a strain rate of over 15 $s^{-1}$. Most other contemporary *in vitro* injury devices cannot attain strain rates of this magnitude. (B) System settings have been changed to produce a deformation lasting 10 s. Note that since strain is applied over a longer duration, the maximum strain rate has decreased to approximately 0.02 $s^{-1}$ and is represented on the right axis in this figure. The experimental data also demonstrates that the shape of the displacement phase and the relaxation phase can be changed independently of each other. (C) All system settings are identical to those in (A) except for the delay between the firing of the vacuum and exhaust solenoid valves. The duration of the strain has been increased from 20 to 90 ms, while other aspects of the strain pulse are unchanged.**

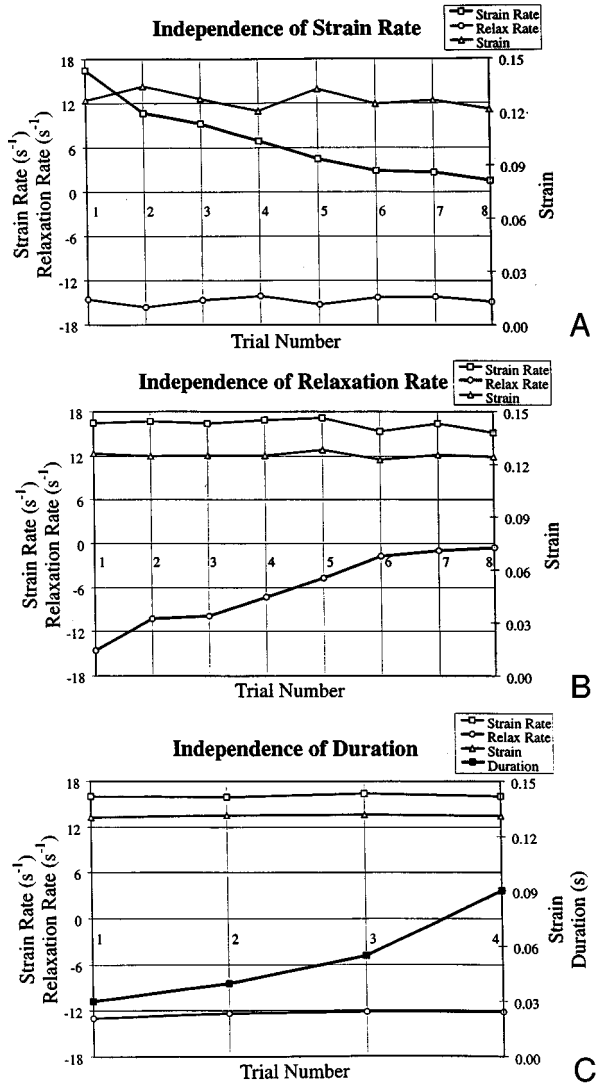


**FIGURE 4. Various aspects of a mechanical stimulus, including strain rate (A), relaxation rate (B), and duration (C), can be changed independently of each other demonstrating the unique control afforded by this device. Strain rate is altered by adjusting the needle valve on the vacuum solenoid; relaxation rate is altered by adjusting the needle valve on the exhaust solenoid; duration is adjusted by altering the delay between activation of the two solenoid valves.**

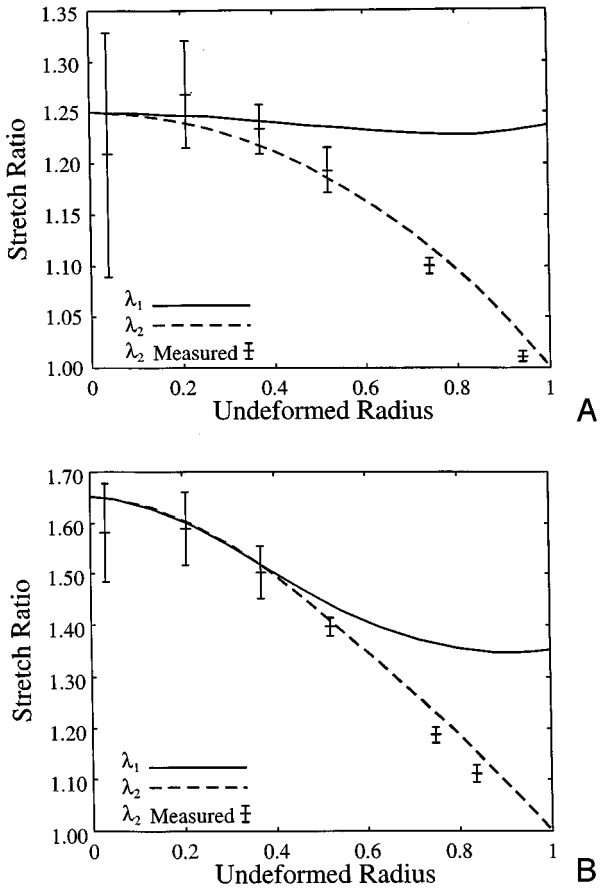


**FIGURE 5. Calculation of the radial and circumferential ($\lambda_1$ and $\lambda_2$, respectively) stretch ratios for center displacements of 5.5 mm (A) and 8 mm (B). Measured circumferential stretch ratios at various points are also included as mean ± SD and show agreement over most of the radial distance. The large standard deviation of the measured strain close to the center of the membrane is due to the precision of the charge-coupled device (CCD) camera used to digitize the membrane and the small size of the inner concentric rings. The precision of the measurements is essentially ±1 pixel which creates a large error in the calculation of strain when the size of the ring is small.**

mula for the biaxial strain at the center of the membrane was in close agreement with the full set of theoretical calculations, underestimating by 0.02 (0.23 vs 0.25) the center strain at a displacement of 5.5 mm.

Due to the hyperelastic strain energy function used to model the Sylgard membrane (see Appendix), the deformation is independent of the modulus of rigidity, **G**. It is of interest to note that the deformation is not dependent upon $\mathbf{k}_1$ below a stretch ratio of 2.00. The deformation is also relatively insensitive to the value of $\mathbf{k}_2$ at stretch ratios less than 1.65.[13] The largest discrepancy in the calculations using extreme values of $\mathbf{k}_2$ ($\mathbf{k}_2 = 0.000$ or $\mathbf{k}_2 = 0.0004$) was a slight change in the radial strain at the edge of the clamped membrane from 0.32 to 0.35.

Membrane casts were made for the following center displacements: 3.1, 3.7, 4.3, 5.5, and 8.0 mm, which correspond to biaxial stretch ratios at the center of 1.08, 1.11, 1.15, 1.25, and 1.65, respectively. The digitized profiles of the casts were superimposed over the calculated membrane profiles (Fig. 6).

## DISCUSSION

The model described herein was based on a type of device which deforms a substrate on which cultured tissue has attached. Substantial improvements were incorporated into the design of the system which reproducibly

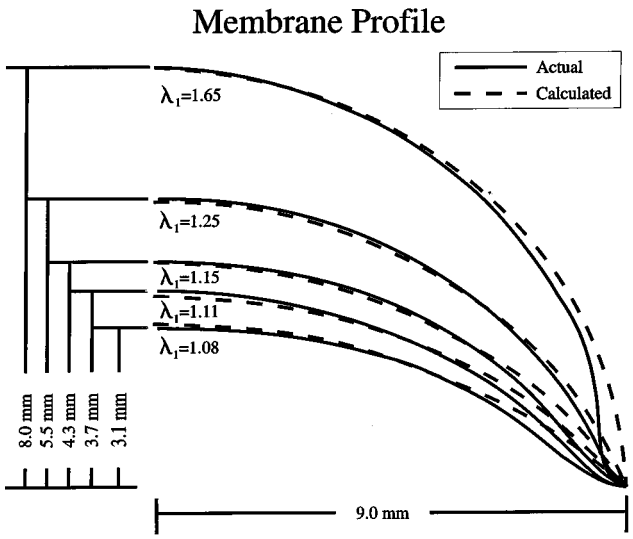


**FIGURE 6. Calculated membrane profiles have been superimposed on experimental membrane profiles digitally traced from casts of deformed membranes. The calculated profiles match the actual profile over much of the membrane radius. The clamped boundary condition produces bending moments at the edge of the membrane which impart the sigmoidal shape.**

generated mechanical stimuli at strains between 0.10 and 0.65, and strain rates as high as 15 $s^{-1}$, which are consistent with those thought to occur in noncontact, inertial head injuries *in vivo*.[9,10,22] This injury device was also designed with the flexibility to mechanically stimulate cultured cells at noninjurious levels so that physiological cellular responses could be compared with pathophysiological responses. The system afforded an unprecedented level of control over the exact shape of the mechanical stimulus via precise and independent control of several parameters including strain, strain rate, relaxation rate, and strain duration. To fully characterize the device, a theoretical analysis of membrane deformation was undertaken. Theoretical results of the membrane profile were compared to casts made of the deformed membrane, while theoretically calculated circumferential strain was compared to measured circumferential strain. Although this information would not be normally available during an experiment, it was acquired in these experiments to validate the strain data output from the device.

The ability to generate high strain rate deformations as well as precisely control those deformations is particularly critical in light of the mechanical properties of brain tissue. The mechanical response of a viscoelastic material such as brain at two different strain rates will differ, and it is likely that the biochemical or cellular response of nervous system tissue subjected to two different strain rates will also differ. Galbraith and colleagues measured the resting potential of the giant squid axon during uniaxial stretch and recovery.[8] It was found that the axon transiently depolarized in response to uniaxial stretch and that as the rate of loading increased, the time required for recovery also increased. Cargill and Thibault found that high strain rate but not quasi-static deformations resulted in an increase in intracellular free calcium in neuroblastoma–glioma cells.[5] LaPlaca and colleagues have found a similar dependence of increased intracellular free calcium on loading rate in a different injury system utilizing terminally differentiated N-tera-2 cells.[17,18] In the same experiments, lactate dehydrogenase release was dependent on loading rate as well. Therefore, the response of biological tissue to injury appears to be sensitive to the rate of loading. Consequently, to elucidate injury mechanisms, it is paramount that tissue be injured in a clinically relevant manner, i.e., at relevant strains and strain rates. The device described herein provides a means of injuring tissue *in vitro* at strains and strain rates similar to those thought to be responsible for nonimpact, inertial head injury *in vivo*.[22,25] It also allows for the precise and independent control of several parameters associated with the injury. This degree of control will be necessary to understand the dependence of the response to injury on the loading rate and the magnitude of the injury.

A substantial improvement associated with this device was the ability to perform noncontact displacement measurement of the membrane during deformation. In other membrane-based devices, membrane deflection has been measured by several means. Although these methods were able to generate rough measurements of membrane displacement, each has inherent limitations. Gorfien and colleagues[11] measured membrane deflection with a stick that rested on the surface of the membrane and moved up and down past a ruler. The stick rested on the membrane of a well that had not been plated with cells and was attached to a manifold of other wells; it was assumed that all wells deformed in an identical manner and that the stick did not affect the deformation. Ellis and colleagues[7] videotaped a membrane as it deformed past a ruler and determined the displacement at intervals of approximately 30 ms. This method cannot be applied to displacements that occur in less than 30 ms. Cargill and Thibault[5] measured the deforming pressure during the injury and later calibrated static displacement to pressure. The displacement during injury is dynamic and is therefore influenced by mass effects associated with the membrane as well as the compressibility of air which are not considered during the static pressure–displacement calibration. Instead of relying on inferred information, the system described herein is capable of measuring the displacement directly with the LDT for every experiment without affecting the deformation of the membrane.

In the present study, the LDT measured backscattered laser light reflected off the target object. Since the exact

nature of the reflected light depends on several factors including surface characteristics of the target, it was necessary to calibrate the LDT for each individual membrane. Because the LDT was calibrated with the membrane in a flat, undeformed position, there was some concern that as the membrane deformed and assumed a curved shape, the laser would be reflected differently, and the original calibration would not be valid. Our results demonstrated that the curvature of the deformed membrane did not affect the calibration of the LDT [Fig. 2(B)]. To demonstrate that the device generates a very reproducible deformation, six deformations, two with each of the three different calibrations, were acquired. The six traces were found to be very similar with a maximum strain discrepancy of approximately 0.02 with a mean of $0.15 \pm 0.007$ (mean$\pm$SD). The overall shape of the strain histories was also very similar with a strain rate of $16.38 \pm 0.70$ and a relaxation rate of $14.39 \pm 0.39$. The data presented in Fig. 2 validate the LDT calibration method and demonstrate that the LDT accurately measures the displacement of the membrane during the insult despite the increase in membrane curvature as it deformed.

In an effort to fully characterize this novel injury device, the strain field across the membrane was calculated. It was assumed that at deflections of $w/a > 3$, the membrane resisted deformation as a membrane and not as a beam.[4,32,38] Measured circumferential strain agreed well with the calculated strain over most of the radius. In addition, the calculated profiles of the displaced membrane agreed with the actual profiles over most of the radius. Discrepancies appeared to be caused by the assumption that the bending moment throughout the membrane was negligible. The effect of the bending moment was most evident at the clamped edge of the membrane and may have been responsible for the discrepancy between calculated and measured strain as well as the sigmoidal shape seen in the actual profiles. Even at $w/a > 20$ (a deflection of 8.0 mm, which is considered to be well into the membrane regime of deformation), edge effects were still evident.[4,36,38] The close agreement of actual to measured values substantiated the choice of a hyperelastic material property for the Sylgard membrane. It appeared as though the deflections of interest here represented a region of transition from purely beam behavior to membrane behavior. The above calculations were valid over most of the radius with the caveat that, due to the bending effects, the solutions may not be valid at the clamped edge. These results suggest that cells or tissue should not be cultured near the edges of the well where the membrane is clamped.

## CONCLUSION

A deeper understanding of both the physical and cellular mechanisms involved in the pathophysiology of brain injury is necessary to more effectively care for the head injured population, and the *in vitro* model described herein may provide new insights. Although *in vitro* models of injury cannot replace *in vivo* models, their major limitations may be, for specific hypotheses, their greatest assets. By employing specifically designed *in vitro* models, it is possible to study a purely mechanical injury in the absence of secondary injury mechanisms, and this model allows for the mechanical insult to be directly measured and precisely controlled. To gain insight into the more complex mechanisms associated with the posttraumatic sequelae, secondary factors can be superimposed on the purely mechanical insult.[5,35] With the aid of greater control afforded by this model over the mechanical insult at large strains and high strain rates, it is hoped that improved tissue tolerance criteria can be developed to better engineer preventative equipment and that by providing the means to better understand the posttraumatic sequelae, management of the traumatically brain-injured patient can be improved.

## ACKNOWLEDGMENTS

We would like to thank Dr. Michelle C. LaPlaca, Dr. Ramesh Raghupathi, and Dr. Kathryn E. Saatman for their helpful comments and critical reading of the manuscript. This work was supported in part, by National Institutes of Health Grant Nos. NINDS-R01-NS26818 and NINDS-P01-NS08803, and a Veterans Administration Merit Review Grant.

## APPENDIX

The theory of elasticity is presented as it applies specifically to circular clamped membranes. If the principle radii of curvature are large compared with the membrane thickness and the stretch ratios are sufficiently large, then the equations of equilibrium may neglect stress variations over the shell thickness. It will further be assumed that the material is homogeneous, isotropic, and incompressible, and is subjected to a pressure acting normal to the membrane at all times.

The material is assumed to behave as a hyperelastic material and is governed by the following strain energy equations:[12]

$$\frac{\partial W}{\partial I_1} = G \exp k_1 (I_1 - 3)^2, \tag{A1}$$

$$\frac{\partial W}{\partial I_2} = \frac{Gk_2}{I_2}, \tag{A2}$$

where $\mathbf{G}$, $\mathbf{k_1}$, and $\mathbf{k_2}$ are material specific parameters. $\mathbf{I_1}$ and $\mathbf{I_2}$ are the first and second invariants of the strain tensor.

The complete set of governing equations may be split into three categories, geometrical, equilibrium, and elasticity considerations.[2,13,15] For the coordinate dependent quantities, a subscript of 1 denotes a line of radius in the undeformed state and a line of longitude in the deformed state; a subscript of 2 denotes a line of circumference in the undeformed and a line of latitude in the deformed state: a subscript of 3 denotes the direction normal to the surface of the membrane.

Dimensional quantities are nondimensionalized as follows and are indicated by a prime notation. Stress resultants, $\mathbf{T_1}$ and $\mathbf{T_2}$, are replaced by $\mathbf{T}_1'$ and $\mathbf{T}_2'$, where

$$T_1' = \frac{T_1}{2hG}, \tag{A3}$$

$$T_2' = \frac{T_2}{2hG}. \tag{A4}$$

All linear dimensions are divided by the characteristic length $\rho_0$, the radius of the clamp, or equivalently, the undeformed membrane. Dimensional pressure is replaced by nondimensional pressure, $\mathbf{P}'$, given by

$$P' = P\,\frac{\rho_0}{2hG}. \tag{A5}$$

The thickness of the undeformed membrane is **h** which appears in the above equations. The radius in the deformed state is **r**. The curvature in the principle directions is represented by $\kappa$, and stretch ratios are represented by $\lambda$.

The deformed geometry is shown in Fig. A1. By definition and by geometrical analysis the following are calculated:

$$\lambda_1 = \frac{ds'}{d\rho'}, \tag{A6}$$

$$\lambda_2 = \frac{r'}{\rho'}, \tag{A7}$$

$$\frac{dr'}{ds'} = \cos\,\theta, \tag{A8}$$

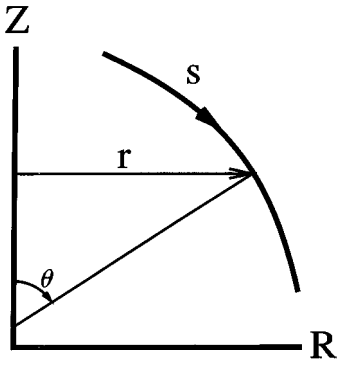


**FIGURE A1. A meridian cross-section of the deformed membrane is presented. The surface S is the surface of the deformed membrane which is axisymmetrical about the Z axis. The deformed radius is depicted by r, and the angle $\theta$ is the angle of declination from the axis of symmetry of the normal to the deformed membrane outer surface.**

$$\kappa_1' = \frac{d\theta}{ds}, \tag{A9}$$

$$\kappa_2' = \frac{\sin\,\theta}{r'}. \tag{A10}$$

By manipulation of the above equations, the following geometric relationships are obtained:

$$\frac{dr'}{d\rho'} = \lambda_1\,\cos\,\theta, \tag{A11}$$

$$\frac{dz}{ds} = -\sin\,\theta, \tag{A12}$$

$$\frac{dr'}{d\rho'} = \lambda_1\sqrt{1-(\kappa_2' r')^2}, \tag{A13}$$

$$\frac{d\lambda_2}{d\rho'} = \frac{1}{\rho'}\left(\frac{dr'}{d\rho'} - \lambda_2\right), \tag{A14}$$

$$\frac{d\kappa_2'}{d\rho'} = \frac{dr'}{d\rho'}\left(\frac{\kappa_1' - \kappa_2'}{r'}\right), \tag{A15}$$

$$\frac{dz'}{d\rho'} = -\lambda_1\kappa_2' r'. \tag{A16}$$

The conditions of equilibrium are ensured by the following equations assuming that the thickness of the membrane is small compared to the curvature:

$$\kappa_1' T_1' + \kappa_2' T_2' = P', \tag{A17}$$

$$2\kappa_2' T_1' = P'. \tag{A18}$$

The first equation specifies equilibrium in the direction normal to the surface of the membrane. The second specifies equilibrium in the axial direction, taking into account the axial symmetry of the deformed membrane as well as the constant internal pressure.

Three elasticity equations can be written which take into account specific material properties:

$$\lambda_3 = \frac{1}{\lambda_1 \lambda_2}, \tag{A19}$$

$$T_1' = \lambda_3(\lambda_1^2 - \lambda_3^2)\left( \exp[k_1(I_1 - 3)^2] + \frac{\lambda_2^2 k_2}{I_2} \right), \tag{A20}$$

$$T_2' = \lambda_3(\lambda_2^2 - \lambda_3^2)\left( \exp[k_1(I_1 - 3)^2] + \frac{\lambda_1^2 k_2}{I_2} \right). \tag{A21}$$

The first equation is dictated by the assumption that the material is incompressible, whereas the specific nature of the other two is dependent upon the hyperelastic nature of the material property. Therefore, the complete state of stress and strain of the membrane is defined by a total of one independent variable ($\rho$) and ten dependent variables, constrained by a system of ten nonlinear equations, (A7) and (A13)–(A21), which can be solved numerically.

## REFERENCES


[1] Adams, J. H., D. I. Graham, L. S. Murray, and G. Scott. Diffuse axonal injury due to nonmissile head injury in humans: An analysis of 45 cases. *Ann. Neurol.* 12:557–563, 1981.

[2] Adkins, J. E., and R. S. Rivlin. Large elastic deformations of isotropic materials IX. The deformation of thin shells. *Philos. Trans. R. Soc. London, Ser. A* 244:505–531, 1952.

[3] Balentine, J. D., W. B. Greene, and M. Bornstein. *In vitro* spinal cord injury. *Lab. Invest.* 58:93–99, 1988.

[4] Brodland, G. W. Highly non-linear deformations of uniformly-loaded circular plates. *Int. J. Solids Struct.* 24:351–362, 1988.

[5] Cargill, R. S., and L. E. Thibault. Acute alterations in $[Ca^{2+}]_i$ in NG 108-15 cells subjected to high strain rate deformation and chemical hypoxia: An *in vitro* model for neural trauma. *J. Neurotrauma.* 13:396–407, 1996.

[6] Christman, C. W., M. S. Grady, S. A. Walker, K. L. Holloway, and J. T. Povlishock. Ultrastructural studies of diffuse axonal injury in humans. *J. Neurotrauma* 11:173–186, 1994.

[7] Ellis, E. F., J. S. McKinney, K. A. Willoughby, S. Liang, and J. T. Povlishock. A new model for rapid stretch-induced injury of cells in culture: Characterization of the model using astrocytes. *J. Neurotrauma* 12:325–339, 1995.

[8] Galbraith, J. A., L. E. Thibault, and D. R. Matteson. Mechanical and electrical responses of the giant squid axon to simple elongation. *J. Biomech. Eng.* 115:13–22, 1993.

[9] Gennarelli, T. A. Animate models of head injury. *J. Neurotrauma* 11:357–368, 1994.

[10] Gennarelli, T. A., L. E. Thibault, J. H. Adams, D. I. Graham, C. J. Thompson, and R. P. Marcincin. Diffuse axonal injury and traumatic coma in the primate. *Ann. Neurol.* 12:564–574, 1982.

[11] Gorfien, S. F., F. K. Winston, L. E. Thibault, and E. J. Macarak. Effects of biaxial deformation on pulmonary endothelial cells. *J. Cell Physiol.* 139:492–500, 1989.

[12] Hart-Smith, L. J. Elasticity parameters for finite deformations of rubber-like materials. *Z. Angew. Math. Phys.* 17:608–626, 1966.

[13] Hart-Smith, L. J., and J. D. C. Crisp. Large elastic deformations of thin rubber membranes. *Int. J. Eng. Sci.* 5:1–24, 1967.

[14] Kirkpatrick, J. B., M. L. Higgins, J. H. Lucas, and G. W. Gross. *In vitro* simulation of neural trauma by laser. *J. Neuropathol. Exp. Neurol.* 44:268–284, 1985.

[15] Klingbeil, W. W., and R. T. Shield. Some numerical investigations on empirical strain energy functions in the large axi-symmetric extensions of rubber membranes. *Z. Angew. Math. Phys.* 15:608–629, 1964.

[16] Koeneman, J. B. Viscoelastic properties of brain tissue. MS thesis, Case Institute of Technology, Cleveland, OH, 1966.

[17] LaPlaca, M. C., V. M. Lee, and L. E. Thibault. An *in vitro* model of traumatic neuronal injury: Loading rate-dependent changes in acute cytosolic calcium and lactate dehydrogenase release. *J. Neurotrauma* 14:355–368, 1997.

[18] LaPlaca, M. C., and L. E. Thibault. An *in vitro* traumatic injury model to examine the response of neurons to a hydrodynamically induced deformation. *Ann. Biomed. Eng.* 25:665–677, 1997.

[19] Lucas, J. H. *In vitro* models of mechanical injury. *J. Neurotrauma* 9:117–121, 1992.

[20] Lucas, J. H., and A. Wolf. *In vitro* studies of multiple impact injury to mammalian CNS neurons: prevention of perikaryal-damage and death by ketamine. *Brain Res.* 543:181–193, 1991.

[21] Margulies, S. S. Biomechanics of traumatic coma in the primate. Ph.D. Thesis, University of Pennsylvania, Philadelphia, PA, 1990.

[22] Margulies, S. S., L. E. Thibault, and T. A. Gennarelli. Physical model simulations of brain injury in the primate. *J. Biomech.* 23:823–836, 1990.

[23] McKinney, J. S., K. A. Willoughby, S. Liang, and E. F. Ellis. Stretch-induced injury of cultured neuronal, glial, and endothelial cells: Effect of polyethelene glycol-conjugated superoxide dismutase. *Stroke* 27:934–940, 1996.

[24] Meaney, D. F. Biomechanics of acute subdural hematoma in the subhuman primate and man. Ph.D. Thesis, University of Pennsylvania, Philadelphia, PA, 1991.

[25] Meaney, D. F., and L. E. Thibault. Physical model studies of cortical brain deformation in response to high strain rate inertial loading. In: International Conference on the Biomechanics of Impacts. Lyon, France: IRCOBI, 1990, pp. 215–224.

[26] Murphy, E. J., and L. A. Horrocks. A model for compression trauma: pressure induced injury in cell cultures. *J. Neurotrauma.* 10:431–444, 1993.

[27] Oppenheimer, D. R. Microscopic lesions in the brain following head injury. *J. Neurol. Neurosurg. Psychiatry* 31:299–306, 1968.

[28] Pamidi, M. R., and S. H. Advani. Nonlinear constitutive relations for human brain tissue. *J. Biomech. Eng.* 100:44–48, 1978.

[29] Press, W. H., S. A. Teukolsky, W. T. Vetterling, and B. P.

Flannery. Statistical description of Data. In: Numerical Recipes in C, the Art of Scientific Computing. Cambridge, MA: Cambridge University Press, 1992, pp. 609–655.
[30] Rand, C. W., and C. B. Courville. Histological changes in the brain in cases of fatal injury to the head. *Arch. Neurol. Psychiatry* 31:526–555, 1934.
[31] Regan, R. F., and D. W. Choi. The effect of NMDA, AMPA/kainate, and calcium channel antagonists on traumatic cortical neuronal injury in culture. *Brain Res.* 633:236–242, 1994.
[32] Reissner, E. On finite deflections of circular plates. In: Proceedings of Symposia in Applied Mathematics of the American Mathematical Society. New York: American Mathematical Society, 1949, pp. 213–219.
[33] Shepard, S. R., J. B. G. Ghajar, R. Giannuzzi, S. Kupferman, and R. J. Hariri. Fluid percussion barotrauma chamber: A new *in vitro* model for traumatic brain injury. *J. Surg. Res.* 51:417–424, 1991.
[34] Shuck, L. Z., and S. H. Advani. Rheological response of human brain tissue in shear. *Trans. ASME, J. Basic Eng.* 12:905–911, 1972.
[35] Tavalin, S. J., E. F. Ellis, and L. S. Satin. Mechanical perturbation of cultured cortical-neurons reveals a stretch-induced delayed depolarization. *J. Neurophysiol.* 74:2767–2773, 1995.
[36] Thibault, L. E., and D. L. Fry. Mechanical characterization of membranelike biological tissue. *J. Biomech. Eng.* 105:31–38, 1983.
[37] Wang, H. C., and A. S. Wineman. A mathematical model for the determination of viscoelastic behavior of brain *in vivo*- I oscillatory response. *J. Biomech.* 5:431–446, 1972.
[38] Williams, J. L., J. H. Chen, and D. M. Belloli. Strain fields on cell stressing devices employing clamped circular elastic diaphrams as substrates. *J. Biomech. Eng.* 114:377–384, 1992.
[39] Winston, F. K., E. J. Macarak, S. F. Gorfien, and L. E. Thibault. A system to reproduce and quantify the biomechanical environment of the cell. *J. Appl. Physiol.* 67:397–405, 1989.